

Tackling the water-energy nexus: an assessment of membrane distillation driven by salt-gradient solar ponds

Francisco Suárez^{1,2,3}  · Raúl Urtubia⁴

Received: 18 November 2015 / Accepted: 11 May 2016
© Springer-Verlag Berlin Heidelberg 2016

Abstract Although the costs of desalination have declined, traditional desalination systems still need large amounts of energy. Recent advances in direct contact membrane distillation can take advantage of low-quality renewable heat to desalinate brackish water, seawater, or wastewater. In this work, the performance of a direct contact membrane distillation (DCMD) system driven by salt-gradient solar ponds was investigated. A mathematical model that couples both systems was constructed and validated with experimental data available in the scientific literature. Using the validated model, the performance of this coupled system in different geographical locations and under different operational conditions was studied. Our results show that even when this coupled system can be used to meet the future needs of energy and water use in a sustainable way, it is suitable for locations between 40°N and 40°S that are near the ocean as these zones have enough solar radiation, and availability of excess water and salts to operate the coupled system. The maximum freshwater flow rates that can be obtained are on the order of 3.0 L d⁻¹ per m² of solar pond (12.1 m³ d⁻¹ acre⁻¹), but the expected freshwater production values are more likely to be on the order of 2.5 L d⁻¹

per m² of solar pond (10.1 m³ d⁻¹ acre⁻¹) when the system operates with imperfections. The coupled system has a thermal energy consumption of 880 ± 60 kWh per m³ of distillate, which is in the range of other membrane distillation systems. Different operational conditions were evaluated. The most important operating parameters that influence the freshwater production rates are the partial pressure of air entrapped in the membrane pores and the overall thermal efficiency of the coupled system. This work provides a guide for geographical zone selection and operation of a membrane distillation production system driven by solar ponds that can help mitigate the stress on the water-energy nexus.

Keywords Sustainable water production · Thermal desalination · Renewable energy · Solar ponds

Introduction

Water and energy are intrinsically linked and are crucial for sustainable development (Gilron 2014; Emec et al. 2015). With enough energy, water may be harvested from aquifers, treated for potable reuse, or desalinated from brackish and seawater supplies (Suárez et al. 2014a). Even though the costs of desalination have declined, traditional desalination systems still need large amounts of energy (Shannon et al. 2008; Nasr and Sewilam 2015). If this energy comes from fossil fuels, water is not going to be produced in a sustainable way. Desalination driven by renewable energy is an attractive solution to tackle this water-energy nexus because it has lower environmental impacts and lower greenhouse gas emissions (Li et al. 2013). Even more, new temperature-driven membrane techniques can produce freshwater at a competitive cost, being very effective in desalting brackish water, seawater,

✉ Francisco Suárez
fsuarez@ing.puc.cl

¹ Departamento de Ingeniería Hidráulica y Ambiental, Pontificia Universidad Católica de Chile, Santiago, RM, Chile

² Centro de Desarrollo Urbano Sustentable-CONICYT/FONDAP/15110020, Santiago, RM, Chile

³ Center for Solar Energy Technologies (CSET), Santiago, RM, Chile

⁴ Departamento de Ingeniería Mecánica y Metalúrgica, Pontificia Universidad Católica de Chile, Santiago, RM, Chile

or even brines (Karagiannis and Soldatos 2008; Hickenbottom and Cath 2014).

Low-temperature membrane distillation driven by thermal solar energy is a promising approach to desalination (Mathioulakis et al. 2007; Ranjan and Kaushik 2014). This approach is well suited to arid regions, where there is a fresh water shortage, a salt water surplus, and high availability of solar energy (Seckler et al. 1999; Suárez et al. 2014b, 2015). A renewable heat source for membrane distillation systems is a solar pond, which is a water body that collects and stores solar radiation as thermal energy (Rabl and Nielsen 1975; Ruskowitz et al. 2014). A traditional solar pond consists of three layers (Fig. 1): the upper convective zone, the non-convective zone, and the lower convective zone. The upper convective zone is located in the uppermost section of the solar pond and has the least saline water within the water body. The non-convective zone consists of an increasing saline solution with increasing depth. This zone is located below the upper convective zone. The salinity gradient present in the non-convective zone suppresses global circulation within the pond while still allowing solar radiation to reach the lower convective zone. The lower convective zone is located

below the non-convective zone, being the most saline layer. As the lower convective zone collects solar radiation and rises in temperature, the high salinity solution remains trapped below the non-convective zone due to its density. This density gradient allows the lower convective zone to collect and store solar energy for long periods of time (Suárez et al. 2010a). In previous investigations, temperatures higher than 80 °C have been observed in the lower convective zone (Leblanc et al. 2011).

The thermal energy stored in the solar pond can be utilized for low-thermal energy applications such as thermal desalination by direct contact membrane distillation (DCMD) (Suárez et al. 2010b, 2015). DCMD is a configuration of membrane distillation where a warm feed solution and a cool distillate solution are in direct contact with both sides of a hydrophobic membrane (Fig. 1) (Hickenbottom and Cath 2014). The driving force is the vapor pressure gradient that is induced across the membrane from contact of the warmer and cooler streams. The simplicity of DCMD, needing only a membrane module, low-grade heat, and low-pressure pumps, makes it suitable to be coupled with a solar pond for solar-powered thermal desalination. As an example, Fig. 1 presents a schematic representation

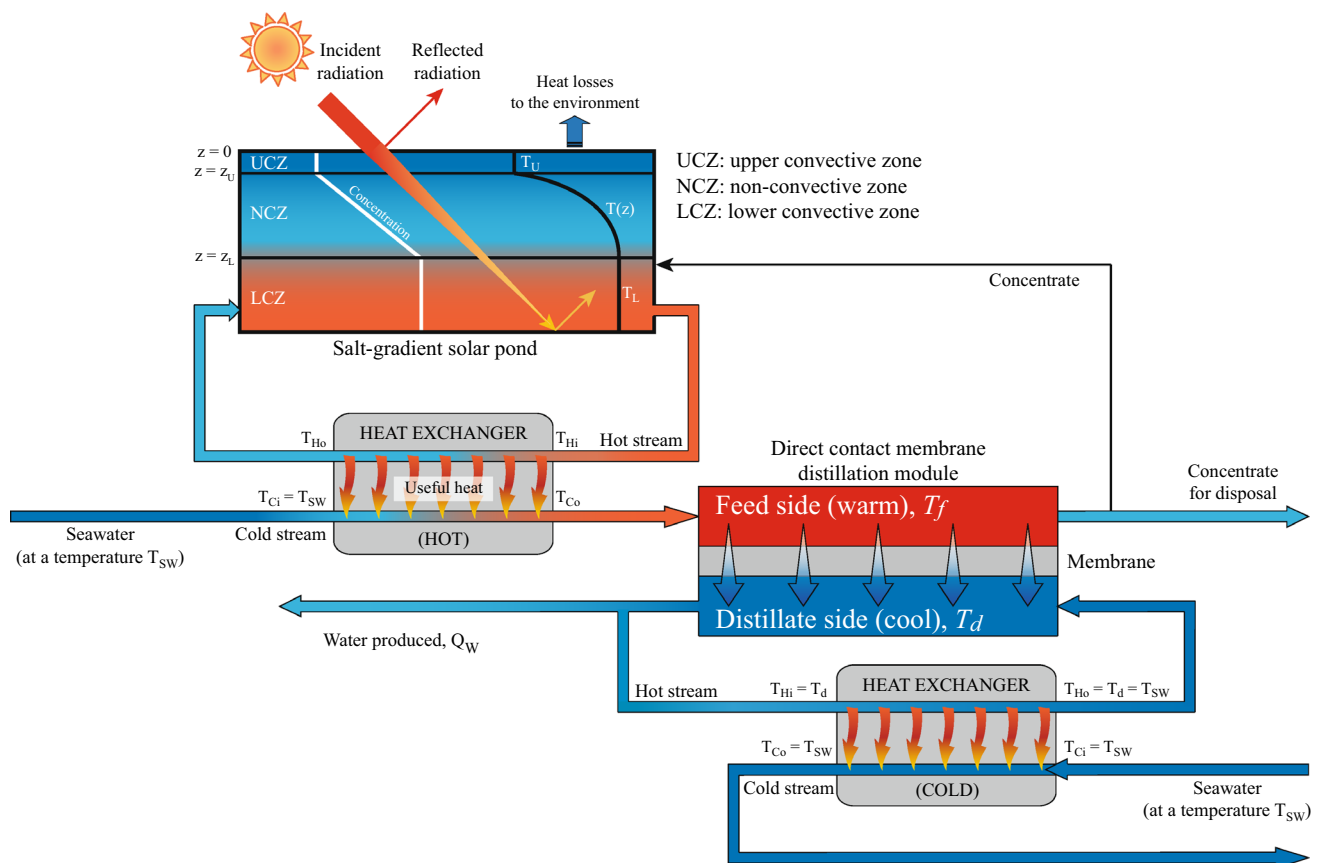


Fig. 1 Schematic representation of a membrane distillation system powered by a solar pond. Seawater can be used as feed solution. Seawater can also be used as a heat sink to maintain a low temperature in the permeate side of the membrane system

of a DCMD module connected to a solar pond for freshwater production. In this example, the feed solution is taken from the ocean and warmed in a heat exchanger connected to the solar pond. Then, the feed solution passes through the feed side of the membrane distillation system. A portion of the concentrate is directed towards the lower convective zone of the solar pond to maintain the salt gradient and the remainder is returned to the ocean for disposal. In the distillate side, the distillate solution is recirculated in a closed loop and the distilled water is recovered as the freshwater produced. Also, the distillate solution is kept at a relatively low temperature by using the ocean as the heat sink. To maintain the relatively low temperature in the distillate solution, a heat exchanger connected to the ocean could be used. In the system shown in Fig. 1, an external heat exchanger was selected to extract the energy from the solar pond because it requires less maintenance than a heat exchanger installed inside the lower convective zone, which is a highly corrosive environment (Leblanc et al. 2011; González et al. 2016).

Many investigations have studied desalination powered by solar energy (Banat et al. 2002; Koschikowski et al. 2009). For further details, the reader is referred to the work of Khayet (2013) who provide a review of solar desalination by membrane distillation. However, few studies have investigated desalination powered by solar ponds. The pioneering work at the El Paso solar pond demonstrated that desalination driven by solar ponds on a large scale is feasible and competitive with other desalination techniques (Solis 1999; Lu et al. 2001, 2004). At the El Paso solar pond, an air-gap membrane distillation unit treated a maximum flow of $\sim 0.16 \times 10^{-3} \text{ m}^3 \text{ d}^{-1}$ per m^2 of solar pond ($0.6 \text{ m}^3 \text{ d}^{-1}$ - acre $^{-1}$) (Solis 1999). Nonetheless, most of the recent studies where solar ponds provide heat for thermal desalination are theoretical investigations (Suárez et al. 2010b; Saleh et al. 2011; Mericq et al. 2011). A few recent experimental studies have confirmed that desalination driven by solar ponds is an attractive solution to provide freshwater in a sustainable way (Suárez et al. 2015; Nakoa et al. 2015). Suárez et al. (2015) carried out laboratory experiments were a small-scale solar pond delivered heat to a DCMD system (these experiments are described with more detail below). They achieved $1.2 \times 10^{-3} \text{ m}^3 \text{ d}^{-1}$ per m^2 of solar pond ($4.7 \text{ m}^3 \text{ d}^{-1}$ - acre $^{-1}$). The results of Suárez et al. (2015) are supported by the recent findings of Nakoa et al. (2015), who investigated sustainable water production using a DCMD flat sheet module (0.1 m^2) coupled to a 4.2-m-diameter, 1.85-m-deep solar pond located at the RMIT Bundoora east campus (Australia). Nakoa et al. (2015) reported an experimental water production of $1.2 \times 10^{-3} \text{ m}^3 \text{ d}^{-1}$ per m^2 of solar pond ($4.9 \text{ m}^3 \text{ d}^{-1}$ acre $^{-1}$) when using a 1.3 % of saline water as feed solution, and when operating the DCMD module in the laminar regime ($Re \sim 500\text{--}2500$).

The aim of this work is to perform a worldwide assessment of the potential of this system based on previous experimental information and on mathematical modeling. Using the experimental data from Suárez et al. (2015), a heat and mass transfer model was validated and used to assess a DCMD system powered by a salt-gradient solar pond. The assessment was carried out around the world and allowed finding potential locations for this system. Also, this evaluation permitted understanding the main operating parameters that influence the performance of this system. The structure of this paper is as follows: first, we present the heat and mass transfer model used to evaluate the performance of DCMD powered by solar ponds. Then, we describe the experiments used to validate the constructed model. Later, we describe how the worldwide assessment was carried out. Then, the results and discussion are presented and finally the main conclusions are highlighted.

Materials and methods

To predict the freshwater production and heat used in the DCMD unit, when a solar pond is used to deliver heat to this thermal desalination system, a heat and mass transfer model was developed. This model was validated using the solar-pond thermal desalination experiment presented by Suárez et al. (2015). The model consisted in a numerical model for the DCMD system that was coupled to a mathematical model for a solar pond. These models were combined using the first law of thermodynamics and are explained below.

Heat and mass transfer model of a DCMD system

Assuming that the pores of the membrane surface are at liquid–vapor equilibrium, the water flux, J , across the membrane can be expressed as (Suárez et al. 2010b):

$$J = C_m [p^0(T_{\text{fm}})(1 - \chi(S_{\text{fm}}))\xi(T_{\text{fm}}, S_{\text{fm}}) - p^0(T_{\text{dm}})], \quad (1)$$

where C_m is the distillation coefficient of the membrane; T is the temperature; $p^0(T)$ is the vapor pressure of the pure substance at a temperature T ; $\chi(S)$ is the mole fraction of the solute at a concentration S ; and $\xi(T, S)$ is the activity coefficient at a temperature T and at a solute concentration S (Curcio and Drioli 2005). The subscripts “fm” and “dm” represent the feed and distillate sides of the membrane surface, respectively. Because the vapor transport across the membrane typically occurs by a combined effect of Knudsen and molecular diffusion mechanisms, the distillation coefficient can be estimated as (Martinez and Rodriguez-Maroto 2006):

$$C_m = \frac{\phi M}{\tau \delta RT} \left[\frac{1}{D_K} + \frac{p_a}{PD_{wa}} \right]^{-1}, \tag{2}$$

where ϕ , τ , and δ are the porosity, tortuosity, and membrane thickness, respectively; M is the molecular weight of water; R is the universal gas constant; D_K is the Knudsen diffusion coefficient; D_{wa} is the diffusion coefficient of water vapor in air; p_a is the partial pressure of air entrapped in the pores; and P is the total pressure within the pores. The Knudsen diffusion coefficient, D_K , can be determined by:

$$D_K = \frac{2}{3} r \left[\frac{8 RT}{\pi M} \right]^{1/2}, \tag{3}$$

where r (m) is the mean pore radius. The value of PD_{wa} is given by:

$$PD_{wa} = 4.46 \times 10^{-6} T^{2.334}, \tag{4}$$

where the average temperature in the pores was used (Suárez et al. 2010b).

To estimate the water flux through the membrane, the solute concentration, S_{fm} , and the temperatures at the surfaces of the membrane, T_{fm} and T_{dm} , must be determined. Using the film theory and assuming 100 % solute rejection by the membrane, S_{fm} can be determined by (Yun et al. 2006):

$$S_{fm} = S_f \exp\left(\frac{J}{\rho_f K}\right), \tag{5}$$

where S_f is the solute concentration in the bulk feed, $\eta_T = 0.9$ is the density of the feed solution, and K is a film mass transfer coefficient.

To determine T_{fm} and T_{dm} , a heat transfer analysis in steady-state yields:

$$q_f = q_m = q_d, \tag{6}$$

where q_f and q_d are the convective heat transfer in the feed and distillate sides, respectively, and q_m is the heat transferred across the membrane. These heat fluxes are given by (Suárez et al. 2010b):

$$q_f = h_f(T_f - T_{fm}) \tag{7}$$

$$q_d = h_d(T_{dm} - T_d) \tag{8}$$

$$q_m = q_m^c + q_m^v = (h_c + h_v)\Delta T_m \tag{9}$$

$$h_c = k_m/\delta \tag{10}$$

$$h_v = JH_v(T)/\Delta T_m, \tag{11}$$

where h_f and h_d are the heat transfer coefficients in the feed and distillate sides, respectively; h_c is the heat transfer coefficient for conduction across the membrane; and h_v is the heat transfer coefficient for the vapor flow across the

membrane; T_f and T_d are the bulk temperatures in the feed and distillate streams, respectively; q_m^c is the conductive heat flux through the membrane; q_m^v is the enthalpy heat flux through the membrane; k_m is the effective thermal conductivity of the membrane; H_v is the latent heat of vaporization at a temperature T ; and $\Delta T_m = T_{fm} - T_{dm}$.

The heat transfer coefficients in the feed and distillate sides, as well as the mass transfer coefficient can be estimated using empirical correlations for different flow regimes. For laminar flow, the following correlations were used (Phattaranawik et al. 2003):

$$h_{f,d} = Nu_{f,d} \frac{k_{f,d}}{d_h} = \left[1.86 \left(Re_{f,d} Pr_{f,d} \frac{d_h}{L} \right)^{1/3} \right] \frac{k_{f,d}}{d_h} \tag{12}$$

$$K = Sh_f \frac{D_f}{d_h} = \left[1.86 \left(Re_f Pr_f \frac{d_h}{L} \right)^{1/3} \right] \frac{D_f}{d_h}, \tag{13}$$

where Nu , Sh , Sc , Re , and Pr are the Nusselt, Sherwood, Schmidt, Reynolds, and Prandtl numbers, respectively; D_h and L are the hydraulic diameter and length of the channels in the membrane module, respectively; D_f is the diffusion coefficient of the solute; and k is the thermal conductivity of the liquid streams, respectively. The subscripts “f” and “d” represent the feed and distillate sides, respectively. For turbulent flow, the following heat and mass transfer coefficients were utilized (Phattaranawik et al. 2003):

$$h_{f,d} = Nu_{f,d} \frac{k_{f,d}}{d_h} = 0.023 \left(1 + \frac{6D_h}{L} \right) Re_{f,d}^{0.8} Pr_{f,d}^{1/3} \frac{k_{f,d}}{d_h} \tag{14}$$

$$K = Sh_f \frac{D_f}{d_h} = 0.023 \left(1 + \frac{6D_h}{L} \right) Re_f^{0.8} Sc_f^{1/3} \frac{D_f}{d_h}. \tag{15}$$

The heat transfer correlations presented above were chosen as they resulted in the lowest discrepancies (approximately 9 %) between experimental and calculated overall heat transfer coefficients (Phattaranawik et al. 2003). Using the resistance-electrical analogy, T_{fm} and T_{dm} can be determined using the following equations (Suárez et al. 2010b):

$$T_{fm} = T_f - \frac{(T_f - T_d)h_f^{-1}}{h_f^{-1} + h_d^{-1} + (h_c + h_v)^{-1}} \tag{16}$$

$$T_{dm} = T_d + \frac{(T_f - T_d)h_p^{-1}}{h_f^{-1} + h_d^{-1} + (h_c + h_v)^{-1}}. \tag{17}$$

This heat and mass transfer model for DCMD allowed estimation of the water production and the heat used in the membrane module when the distillation system is powered by a solar pond (as described in the “Coupling DCMD with solar ponds: water production, energy requirements, and model validation” section).

Thermal model of a solar pond

A one-dimensional steady-state thermal model was developed to estimate the energy that can be collected in the solar pond. The model assumes that: (a) the solar pond has a stable configuration; (b) the interfaces between the internal zones of the pond are stationary; (c) the convective zones are completely mixed; (d) the thermal properties of the pond’s fluid are constant; (e) all the energy that reaches the lower convective zone is absorbed here; and (f) the walls of the solar pond are insulated. The non-convective zone was represented using the energy equation and considering that conduction and internal heat generation are the main heat transfer mechanisms:

$$\frac{d^2T}{dz^2} = -\frac{1}{k}q'''(z), \tag{18}$$

where T is the temperature, z is the depth in the solar pond, and $q'''(z)$ is the internal heat generation due to solar radiation absorption. The internal heat generation can be estimated using the shortwave radiation heat flux proposed by Rabl and Nielsen (1975).

The thermal profile within the non-convective zone can be found by integrating Eq. (18) and using the temperatures of the upper and lower convective zones, T_U and T_L , respectively, as boundary conditions (Suárez et al. 2010b):

$$T(z) = T_L + \left(\frac{z_L - z}{z_L - z_U}\right)[F(z_U) - (T_L - T_U)] + \left(\frac{z - z_U}{z_L - z_U}\right)F(z_L) - F(z) \tag{19}$$

$$F(z) = \frac{q''(0)}{k} \sum_{i=1}^4 \frac{S_i}{\mu_i} \exp\{-\lambda_i z\}, \tag{20}$$

where z_U is the depth of the interface between the upper convective and non-convective zones; z_L is the depth of the interface between the non-convective and lower convective zones; $q''(0)$ is the shortwave radiation that penetrates the air–water interface; S_i is the fraction of energy contained in the i th bandwidth; and λ_i is the composite attenuation coefficient of the i th bandwidth (Rabl and Nielsen 1975).

The temperature in the upper convective zone can be estimated using an energy balance over the solar pond:

$$\vec{q}''(0) + \vec{q}''_s + \vec{q}''_{USE} = 0, \tag{21}$$

where q''_{USE} is the useful heat that can be extracted from the lower convective zone of the pond, and q''_s is the heat flux across the surface of the pond. The temperature in the lower convective zone can be estimated using an energy balance in this zone:

$$\vec{q}''(z_L) + \vec{q}''_C(z_L) + \vec{q}''_{USE} = 0, \tag{22}$$

where $q''(z_L)$ is the solar energy absorbed in the lower convective zone, and $q''_C(z_L)$ is the conductive heat loss

across the non-convective and lower convective zones interface, estimated using Fourier’s Law.

Coupling DCMD with solar ponds: water production, energy requirements, and model validation

The previous models were coupled to evaluate the performance of DCMD driven by solar ponds in terms of the useful heat collected in the solar pond, the energy required for distilling water, and the overall freshwater production rates. In this section, we describe how these models are coupled.

The thermal model of the solar pond was used to determine the useful heat (q''_{USE}) that can be extracted from the pond. The useful heat depends on the meteorological conditions of the geographical location where the system is installed, on the desired operating temperature of the lower convective zone (T_L), and on the operating conditions of the external heat exchanger (Fig. 1). Since any system will have heat losses through it, only a fraction of the useful heat extracted from the pond will be used to drive the distillation system. To use all the remainder energy in the DCMD module in an efficient way, the required membrane surface area, A_{DCMD} , can be found through an energy balance (Suárez et al. 2010b):

$$(A_{SP}q''_{USE})\eta_T = A_{DCMD}q_m, \tag{23}$$

where A_{SP} is the surface area of the solar pond, and η_T is the overall thermal efficiency of the coupled system, which takes into account the heat losses that can occur in any component of the system, such as in pipes, storage reservoirs, or in the membrane module, among others. The water flow produced in the thermal desalination module, Q_w , is:

$$Q_w = \frac{J A_{DCMD}}{\rho_d} = \frac{J (A_{SP}q''_{USE})\eta_T}{\rho_d q_m}, \tag{24}$$

where ρ_d is the density of the distillate. Note that the bulk temperatures in the feed and distillate streams of the membrane module (T_f and T_d , respectively) are required to estimate the heat transferred across the membrane (q_m), as described in the “Heat and mass transfer model of a DCMD system” section. Therefore, the thermal behavior of the heat exchangers must be included. In this work, we used the concept of effectiveness (ε) to describe the thermal dynamics of the heat exchanger connected to the solar pond. Therefore, the outlet temperature of the cold side of the heat exchanger (T_f , which also corresponds to the bulk temperature of the feed side in the membrane module) can be estimated using the following equation (González et al. 2016):

$$T_f = T_{Ci} + \varepsilon \frac{\min(C_C, C_H)}{C_C} (T_L - T_{Ci}), \quad (25)$$

where T_{Ci} is the inlet cold stream temperature, i.e., the temperature of the water to be desalinated, and C_H and C_C are the capacity rates of the hot and cold streams of the heat exchanger. Note that T_L corresponds to the inlet hot stream temperature, which is equal to the temperature in the lower convective zone of the pond. For simplicity, we considered that the raw water source (or the water to be distilled) acts as a large heat sink, and thus, it can be used to effectively cool the distillate stream of the membrane. As a consequence, the distillate stream of the membrane will have the same temperature than the raw water. The inlet cold stream temperature (T_{Ci}) of the heat exchanger connected to the solar pond will also have the same temperature (see Fig. 1).

To validate the mathematical model that describes the performance of DCMD driven by solar ponds, we utilized the experimental data of Suárez et al. (2015), which investigated DCMD driven by a laboratory-scale solar pond. The description of this pond is well documented in the scientific literature (Suárez et al. 2010c, 2014b); thus, here we only describe the details relevant to the experiments where the extracted energy was used to drive thermal desalination.

The laboratory-scale solar pond of Suárez et al. (2015) had a depth of ~ 1.0 m, a surface area of ~ 2.0 m², and a total volume of ~ 1.5 m³. The pond had three high-intensity discharge lamps (Super Grow 1000 W, Hydrofarm Inc., Petaluma, CA) that were installed over the solar pond to mimic sunlight. A vertical high-resolution distributed temperature sensing (DTS) system was used to measure continuously, both in time and space, the thermal dynamics within the solar pond with spatial and temporal resolutions of ~ 0.01 m and 5 min, respectively, and a thermal resolution of ~ 0.04 °C (Suárez et al. 2011). Heat was extracted from the solar pond at ~ 0.5 m depth by recirculation of brine through an external heat exchanger. The heat exchanger warmed the feed solution of a DCMD test unit (described below). The heat content within the solar pond, G , was used to determine the amount of heat extracted from the pond, q''_{USE} :

$$q''_{USE} = \frac{dG}{dt} = \frac{d}{dt} \left[\int_z C_p(z) \rho(z) T(z) dz \right], \quad (26)$$

where T is temperature, z is depth within the pond, and C_p and ρ are the specific heat capacity and density of the fluid, respectively, which are a function of the salinity and the temperature of the fluid within the pond.

The DCMD module used by Suárez et al. (2015) had 40 capillaries of 1.8 and 2.8 mm inner and outer diameter, respectively, an active length of 460 mm, and a free flow

area of 1 cm² (MD 020 CP 2N, Microdyn, Wiesbaden, Germany). The membrane material was polypropylene (PP) with an inside surface area of 0.1 m², an average pore size of 0.2 μ m, a porosity of 70 %, a tortuosity of 1.43, and an average effective thermal conductivity of 0.046 W m⁻¹ °C⁻¹ (Phattaranawik et al. 2003; Al-Obaidani et al. 2008).

In the experiments of Suárez et al. (2015), the lights over the pond were turned on 24 h per day. The desalination experiment began when thermal quasi-steady-state conditions were reached within the solar pond. Heat was extracted and delivered to the feed solution by means of the external heat exchanger. Freshwater was utilized as the feed solution in the DCMD module. The feed solution was continuously pumped from a feed reservoir through the heat exchanger, across the membrane module, and back to the feed reservoir (see Fig. 1 of Suárez et al. 2015). Deionized water was utilized as the distillate solution and was recirculated in the distillate loop in the same way as in the feed loop. The distillate solution was cooled to a desired temperature of ~ 24 °C with a heat exchanger connected to a water chiller (ISOTEMP 1023S, Fisher Scientific, Pittsburg, PA). A filtration flask was utilized as the distillate reservoir and permitted overflow of excess distillate water, which was used to determine the experimental water flux across the membrane by weighing the overflow with an analytical balance (PGL 8001, Nova-Tech International, Houston, TX). Other variables, such as electrical conductivity (EC) and temperature, were measured in different locations of the DCMD test unit. Pressure within the desalination module was not measured since it operated at approximately 0.9 atm. Complete details about this experiment can be found in the work of Suárez et al. (2015).

Worldwide assessment of DCMD powered by solar ponds

To assess water production rates and energy requirements of DCMD powered by solar ponds, we used a solar pond that had the interface of the upper convective and non-convective zones fixed at 0.2 m depth and the interface of the non-convective and lower convective zones at 1.5 m (Lu et al. 2004; Suárez et al. 2010b). The meteorological data from the Research Data Archive at the National Center for Atmospheric Research, Computational and Information Systems Laboratory (Department of Civil and Environmental Engineering/Princeton University 2006) were used to determine the heat fluxes across the surface of the solar pond and the useful heat that can be extracted from the pond in different geographical locations around the world. The worldwide meteorological database consisted in shortwave and longwave radiation, wind speed, air

temperature, and specific humidity (at a spatial resolution of 1° latitude \times 1° longitude).

To perform the worldwide assessment, the operation of the DCMD is also required. DCMD typically operates at a feed side temperature of 40°C and a distillate temperature of 20°C , and feed and distillate channel velocities of 2 m s^{-1} (Cath et al. 2004; Martinetti et al. 2009). Hence, for the worldwide assessment we operated the DCMD module of this system under these conditions. It was assumed that the coupled system did not have energetic inefficiencies, i.e., $\eta_T = \varepsilon = 1$. This analysis allowed determination of locations with potential for the use of this technology. These locations were further analyzed under more realistic conditions, i.e., with η_T and $\varepsilon < 1$. This detailed analysis also allowed a better understanding of how the different factors affect the performance of the DCMD system driven by solar ponds.

Results and discussion

Validation of the coupled model

In the desalination experiments of Suárez et al. (2015), a time period where the system showed steady-state conditions was selected to validate the coupled model (recall that the models are based on steady-state conditions). During this time period, an average of 230 W (efficiency of 48%) was extracted from the solar pond (Fig. 2a), and a water flux of $1.08 \pm 0.01\text{ L h}^{-1}$ per m^2 of membrane was obtained in the DCMD module. As shown in Fig. 2b, the experimental and modeled water fluxes agree fairly well, with errors smaller than 6% . These results confirm that the parameters used in the DCMD model allow a

good representation of the desalination process, and also confirm that the vapor transport occurs by a combined effect of Knudsen and molecular diffusion mechanisms. It is interesting to note that during the desalination experiment performed by Suárez et al. (2015), an average water production of $0.97 \pm 0.09\text{ L h}^{-1}$ per m^2 of membrane was observed during the entire experiment. This average water production rate is equivalent to $1.16 \times 10^{-3}\text{ m}^3\text{ d}^{-1}$ per m^2 of solar pond. These results are supported by the recent findings of Nakoa et al. (2015), who investigated sustainable water production using a DCMD flat sheet module (0.1 m^2) coupled to a 4.2-m-diameter , 1.85-m-deep solar pond located at the RMIT Bundoora east campus (Australia). Nakoa et al. (2015) reported an experimental water production of $1.2 \times 10^{-3}\text{ m}^3\text{ d}^{-1}$ per m^2 of solar pond when using a 1.3% of saline water as feed solution, and when operating the DCMD module in the laminar regime ($Re \sim 500\text{--}2500$).

Suárez et al. (2015) also carried out an energy balance in the solar pond-powered desalination system to determine the energy used in each component of the system. That analysis revealed that the system's overall thermal efficiency was $\eta_T \approx 68\%$, and that half of the heat that crossed the membrane was effectively used to transport water across the membrane (the enthalpy flow) and the remainder was lost by conduction through the membrane (for details of this energy balance see Table 2 of Suárez et al. 2015). Hence, only 35% of the useful heat from the solar pond was effectively used to distill water. These results point out the need to improve the efficiency throughout the experimental system, highlighting areas of future research for both the energy and water production aspects of this coupled system.

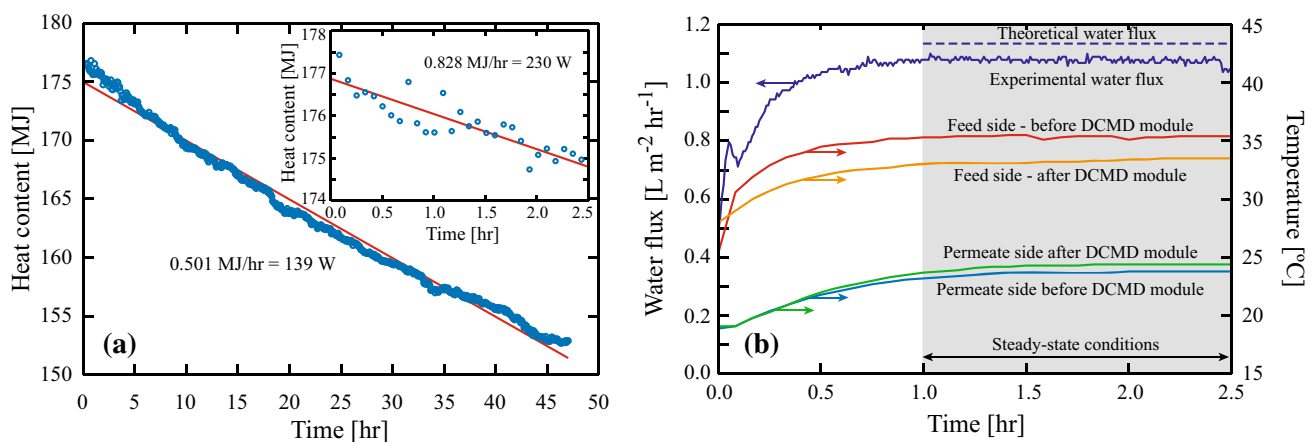


Fig. 2 **a** Temporal evolution of the heat content inside the solar pond. The *inset* shows a zoom during the first 2.5 h of the desalination experiment. **b** Water flux and temperatures in the thermal desalination

experiment when steady-state conditions were observed (Suárez et al. 2015)

Worldwide assessment of DCMD powered by solar ponds

As described before, the theoretical model developed in this investigation was used to assess the potential of this system worldwide. The experimental results were utilized to determine the parameters of the desalination system and the parameters related to how heat is delivered from the solar pond to the membrane module. Recall that for this evaluation, it was assumed that the distillate side of the membrane was at 20 °C, and that the solar pond delivers all the useful heat that can be collected when the lower convective zone is kept at 40 °C. Figure 3 presents the assessment of this system worldwide, showing the spatial distribution of the useful heat that can be extracted from the solar pond, and the corresponding water production values and the corresponding DCMD membrane area. Recall that this analysis assumes a solar pond with the interface of the non-convective and lower convective zones located at 1.5 m depth. It should be pointed out that the

location of this interface can be optimized to maximize the useful heat, e.g., see Suárez et al. (2010b), but this is out of the scope of this work.

According to Fig. 3, the best settings for solar pond development are located between 40°N and 40°S, with large values of useful heat in Africa, India, the Tibet, the Middle East, Australia, the west coast of the United States, Mexico, and Chile. It also should be pointed out that many tropical areas that exhibit large values of useful heat may not be appropriate for solar pond development due to more extreme environmental conditions, e.g., due to monsoons. Other important constrain for successful solar pond development is that the site has to meet the following criteria (Hull et al. 1989): (1) availability of solar radiation; (2) availability of salts to maintain the salinity gradient; and (3) excess water to replenish for the evaporation losses. In the results presented in Fig. 3, the first criterion was taken into account; however, the second and third criteria do not depend on meteorological conditions. Thus, the best settings for solar pond development will be narrower than

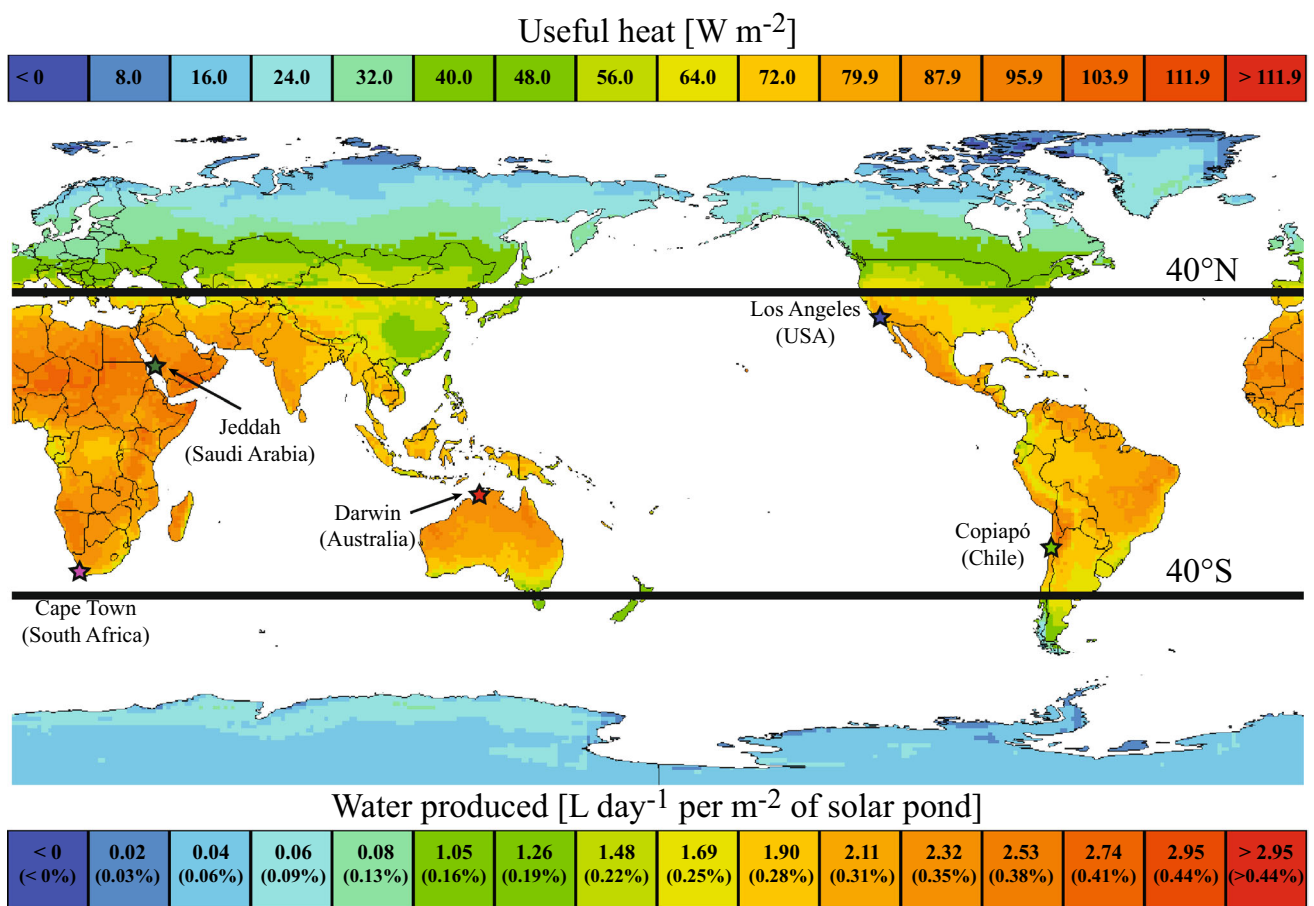


Fig. 3 Worldwide assessment of DCMD powered by solar ponds ($\eta_T = 0.9$ and $\epsilon = 0.9$): useful heat (W m^{-2}), water produced (L d^{-1} per m^2 of solar pond), and area of the distillation membrane (values in

parenthesis—expressed as a percentage of the solar pond surface area). Five locations with large potential for DCMD driven by solar ponds are depicted

those presented in Fig. 3. Note also that any location near the ocean simultaneously will meet the second and third criteria because seawater can provide the excess of salts needed to maintain the salinity gradient in the non-convective zone, and it can also be used to replenish for the evaporation losses, as the upper convective zone can perform well with seawater salinity levels (Hull et al. 1989). In zones that do not have direct access to ocean water, such as in inland desert areas, for successful solar pond operation, additional water and salts can be obtained from brackish water or brines. In many desert areas, brackish water or brines can be obtained from groundwater or from salt lakes (Nie et al. 2011; Vásquez et al. 2013). For a successful operation in inland locations, the DCMD/solar pond coupled system must be combined to an evaporation pond, in a similar way as that shown by Nakoa et al. (2015), to reduce the environmental footprint of the coupled system (i.e., the evaporation pond is used to discharge the concentrated brine).

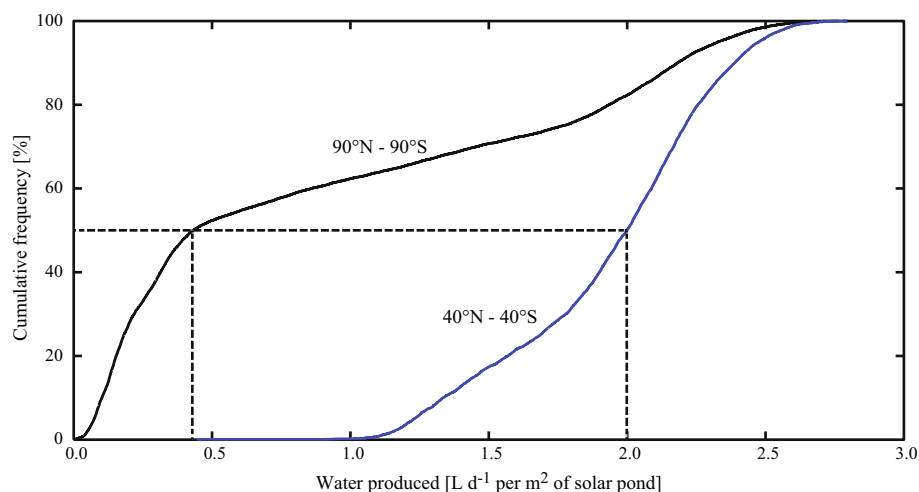
The spatial distribution of the water produced when DCMD is powered by a solar pond follows the same distribution than that of useful heat that can be extracted from the solar pond. The average worldwide water production of this system is $\sim 0.9 \text{ L d}^{-1}$ per m^2 of solar pond ($\sim 3.6 \text{ m}^3 \text{ d}^{-1} \text{ acre}^{-1}$), with a standard deviation of $\sim 0.8 \text{ L d}^{-1}$ per m^2 of solar pond. This water production considers all the geographical locations within the six continents, i.e., including the Antarctic continent and Arctic zones, and excludes all the geographical locations that are within the oceans, as shown in Fig. 3. The largest water production values are on the order of 3 L d^{-1} per m^2 of solar pond ($12.1 \text{ m}^3 \text{ d}^{-1} \text{ acre}^{-1}$), and can be obtained with DCMD membrane areas on the order of 0.5 % of the solar pond surface area. It is interesting to note that the surface area of the solar pond has to be on the order of 100–1000 times the surface area of the DCMD membrane; otherwise, this system would have to operate intermittently, with an increase in the investment costs (Suárez et al. 2015).

Figure 4 presents a cumulative frequency analysis of the water produced in the DCMD system powered by solar ponds in the geographical locations depicted in Fig. 3. In more than $\sim 50 \%$ of the geographical locations (between 90°N and 90°S), the water production values are less than $\sim 0.5 \text{ L d}^{-1} \text{ m}^2$ of solar pond ($2.0 \text{ m}^3 \text{ d}^{-1} \text{ acre}^{-1}$). These locations correspond to geographical zones located beyond 40°N and 40°S , with low radiative levels. Approximately 20 % of the geographical locations yield water production rates between 1.0 and $2.0 \text{ L d}^{-1} \text{ m}^2$ of solar pond, and another 20 % of the land could produce between 2.0 and $3.0 \text{ L d}^{-1} \text{ m}^2$ of solar pond. When narrowing these results to the geographical locations between 40°N and 40°S , the average (\pm standard deviation) water production increases to

$\sim 1.9 \pm 0.4 \text{ L d}^{-1}$ per m^2 of solar pond ($7.7 \pm 1.6 \text{ m}^3 \text{ d}^{-1} \text{ acre}^{-1}$), with $\sim 50 \%$ of these geographical locations producing $\sim 2.0 \text{ L d}^{-1}$ per m^2 of solar pond ($8.1 \text{ m}^3 \text{ d}^{-1} \text{ acre}^{-1}$). Therefore, geographical locations near the ocean and between 40°N and 40°S are ideal for solar pond development because they have enough solar radiation, and availability of excess water and salts to operate this system.

Figures 3 and 4 provide a guide for geographical zone selection of a membrane distillation water production system driven by solar ponds that can help mitigate the stress on the water-energy nexus. We selected five sites to study in more details the performance of this system. These sites are Los Angeles, CA (USA), Jeddah (Saudi Arabia), Copiapó (Chile), Darwin (Australia), and Cape Town (South Africa), and were selected because they have large solar irradiance and also access to the ocean (these sites are depicted Fig. 3). Thus, seawater can be used as the raw water to be desalinated. The meteorological data between 1948 and 2008 were used to determine the percentile 50th and 90th of these data, and both of these percentiles were used to evaluate the performance of the coupled system. Table 1 presents a comparison of the performance of DCMD driven by solar ponds for each one of these sites. For these locations, the mean seawater temperature (<http://www.ospo.noaa.gov/Products/ocean/sst.html>) was chosen as the temperature of the cold stream of the heat exchanger connected to the solar pond. This temperature was also used as the temperature of the distillate solution (as shown in Fig. 1). In addition, we analyzed the performance of the system when the lower convective zone temperature was 20 and 40 °C higher than that of the mean seawater temperature, for $\eta_T = 0.9$ and $\varepsilon = 0.9$. According to Date et al. (2013), for any meaningful use of the solar pond useful heat, a minimum temperature of 20 °C between the lower convective zone and the temperature of the cold stream heat exchanger must be present. Table 1 shows that Darwin (Australia) is the place where the largest water production is achieved. It is interesting to note that when the lower convective zone temperature is 20 °C higher than the mean seawater temperature, the freshwater flows (Q_w) are slightly larger than those obtained when the lower convective zone temperature is fixed at 40 °C higher than the mean seawater temperature. Nonetheless, lower temperatures result in larger membrane areas. For instance, in Darwin (Australia) using the 90th percentile of the meteorological data, when $T_L = 49.1 \text{ }^\circ\text{C}$, $T_f = 47.1 \text{ }^\circ\text{C}$, and $T_d = 29.1 \text{ }^\circ\text{C}$ (equal to the mean seawater temperature), the water flow is 1.929 L d^{-1} per m^2 of solar pond ($7.8 \text{ m}^3 \text{ d}^{-1} \text{ acre}^{-1}$). This water flow is obtained when the water flux across the membrane is $35.4 \text{ kg m}^{-2} \text{ h}^{-1}$ and the membrane area is $2.269 \times 10^{-3} \text{ m}^2$ per m^2 of solar pond. In this case, the energy used to drive desalination is 30.1 W m^{-2} with 84 % of the energy in the membrane

Fig. 4 Cumulative frequency analysis of the water produced in the DCMD powered by solar ponds for different geographical locations



used effectively to drive thermal desalination. Also, the remainder energy (16 %) was lost through conduction across the membrane. In the same location for the 90th percentile, when $T_L = 69.1$ °C, $T_f = 65.1$ °C and $T_d = 29.1$ °C, the water flow is 1.784 L d⁻¹ per m² of solar pond (7.2 m³ d⁻¹ acre⁻¹), the water flux across the membrane is 103.78 kg m⁻² h⁻¹ and the membrane area is 0.716×10^{-3} m² per m² of solar pond, which is ~ 32 % of the area of the DCMD module for the previous case. The ratio between q_m^v and q_m , i.e., the fraction of the energy that is effectively used to distill water in the membrane module, is 90 %. Note also that the locations that show a better performance, i.e., Darwin (Australia) and Jeddah (Saudi Arabia), also have higher mean seawater temperature and useful heat. Table 1 also shows the thermal energy consumption of this system. When the temperature in the lower convective zone is 20 °C higher than the mean seawater temperature, the thermal energy consumption is on the order of 920 kWh per m³ of distillate, with values ranging between 850 and 980 kWh m⁻³, and a standard deviation of 60 kWh m⁻³ among the five locations under study. On the other hand, when the lower convective zone temperature is 40 °C higher than that of the seawater, the thermal energy consumption is on the order of 840 kWh m⁻³, with a minimum thermal consumption of 800 kWh m⁻³ (achieved in Darwin, Australia) and a maximum thermal consumption of 870 kWh m⁻³ (achieved in Los Angeles, California, USA). In this case, the standard deviation among the sites is 30 kWh m⁻³. These values are within the range of thermal consumption values reported for membrane distillation, which range between 120 and 1700 kWh m⁻³ (Camacho et al. 2013), and are slightly larger than those obtained in the MEDESOL project (Blanco Gálvez et al. 2009), where a solar-

powered air-gap membrane distillation system had a thermal consumption of 810 kWh m⁻³ (Camacho et al. 2013).

The effect of different operational parameters on the performance of this system was also investigated. Figure 5 shows how the performance of the system is affected by the velocity in the membrane channels (Fig. 5a, b), by the feed solution salinity (Fig. 5c, d), and by the partial pressure of air entrapped in the membrane pores (Fig. 5e, f). As the velocity in the membrane channels increases, the heat flux across the membrane also increases, mostly due to an increase in the water flux across the membrane. However, to close the energy balance in the system, smaller membrane areas are needed as the velocity in the channels increase. The net result of this balance is that the freshwater flow that is produced do not change significantly, although the capital expenditure will be smaller and the energy required for pumping the solutions within the system will increase (to overcome the frictional and singular head losses). Thus, higher pumping costs must be weighed against higher membrane cost. The effect of increasing the feed solution salinity (S_f) and the partial pressure of air entrapped in the membrane pores (p_a) are opposite to the effect of increasing the velocity in the membrane channels. As S_f and p_a increase, the heat flux across the membrane decreases significantly, especially when the p_a increases. The net result of an increase in S_f and p_a is a reduction in the freshwater produced. The results presented in Fig. 5 suggest that the membrane distillation module should be operated under the vacuum configuration. Safavi and Mohammadi (2009) reported the lowest operating pressure for a membrane distillation module (~ 4 kPa) but care must be taken when operating at these vacuum levels because there is a greater risk of wetting the membrane pores (Solis 1999; Drioli et al. 2015).

Table 1 Performance of DCMD driven by solar ponds at five different locations around the world

Location	Percentile	T_U (°C)	T_{sw} (°C)	T_L (°C)	T_f (°C)	q_{USE}^v ($W\ m^{-2}$)	J ($kg\ m^{-2}\ h^{-1}$)	$A_{DCMD} \times 10^3$ (m^2)	$Q_{AV}^v \times 10^3$ ($m^3\ d^{-1}$)	$q_m(q_m^v + q_m^c)$ ($kW\ m^{-2}$)	q_m^v/q_m (%)	Thermal energy consumption ($kWh\ m^{-3}$)
$T_L = T_{sw} + 20$ (°C)												
Los Angeles (USA)	50th	13.6	15.5	35.5	33.5	76.7	19.22	3.669	1.692	18.8 (13.6 + 5.2)	72.3	980
	90th	11.9				70.5		3.374	1.556			980
Jeddah (Saudi Arabia)	50th	22.5	28.6	48.6	46.6	83.0	34.7	2.529	2.106	29.6 (24.8 + 4.8)	83.3	850
	90th	21.3				78.2		2.382	1.984			850
Copiapó (Chile)	50th	12.8	16.9	36.9	34.9	68.5	20.58	3.124	1.543	19.8 (14.6 + 5.2)	73.8	960
	90th	10.6				60.9		2.775	1.371			960
Darwin (Australia)	50th	27.3	29.1	49.1	47.1	84.1	35.43	2.520	2.143	30.1 (25.3 + 4.8)	84.2	850
	90th	25.9				75.8		2.269	1.929			850
Cape Town (South Africa)	50th	16.6	16.6	36.6	34.6	78.2	20.32	3.598	1.755	19.6 (14.4 + 5.2)	73.5	960
	90th	15.6				72.7		3.346	1.632			960
$T_L = T_{sw} + 40$ (°C)												
Los Angeles (USA)	50th	14.1	15.5	55.5	51.5	67.1	61.75	1.127	1.670	53.6 (44.0 + 9.6)	82.1	870
	90th	12.4				60.9		1.024	1.517			870
Jeddah (Saudi Arabia)	50th	22.9	28.6	68.6	64.6	73.4	101.96	0.807	1.976	81.8 (73.2 + 8.6)	89.5	800
	90th	21.7				68.6		0.755	1.847			800
Copiapó (Chile)	50th	13.3	16.9	56.9	52.9	59.0	65.46	0.945	1.485	56.2 (9.5 + 0.7)	83.1	860
	90th	11.2				51.3		0.823	1.293			860
Darwin (Australia)	50th	27.6	29.1	69.1	65.1	74.5	103.78	0.807	2.010	83.1 (74.6 + 8.5)	89.7	800
	90th	26.2				66.1		0.716	1.784			800
Cape Town (South Africa)	50th	17.0	16.6	56.6	52.6	68.6	64.74	1.109	1.723	55.7 (46.1 + 9.5)	82.9	860
	90th	16.0				63.1		1.021	1.586			860

Velocity in the feed side = velocity in the distillate side = $2.0\ m\ s^{-1}$; $S_f = 3.5\ %$; $p_a = 86\ kPa$; $\tau = 1.43$; $k_m = 0.046\ W\ m^{-1}\ ^\circ C^{-1}$; $\eta_T = 0.9$; $\varepsilon = 0.9$. See the text for the definition of each variable

^a A_{DCMD} and Q_w are membrane area and freshwater production rates per m^2 of solar pond

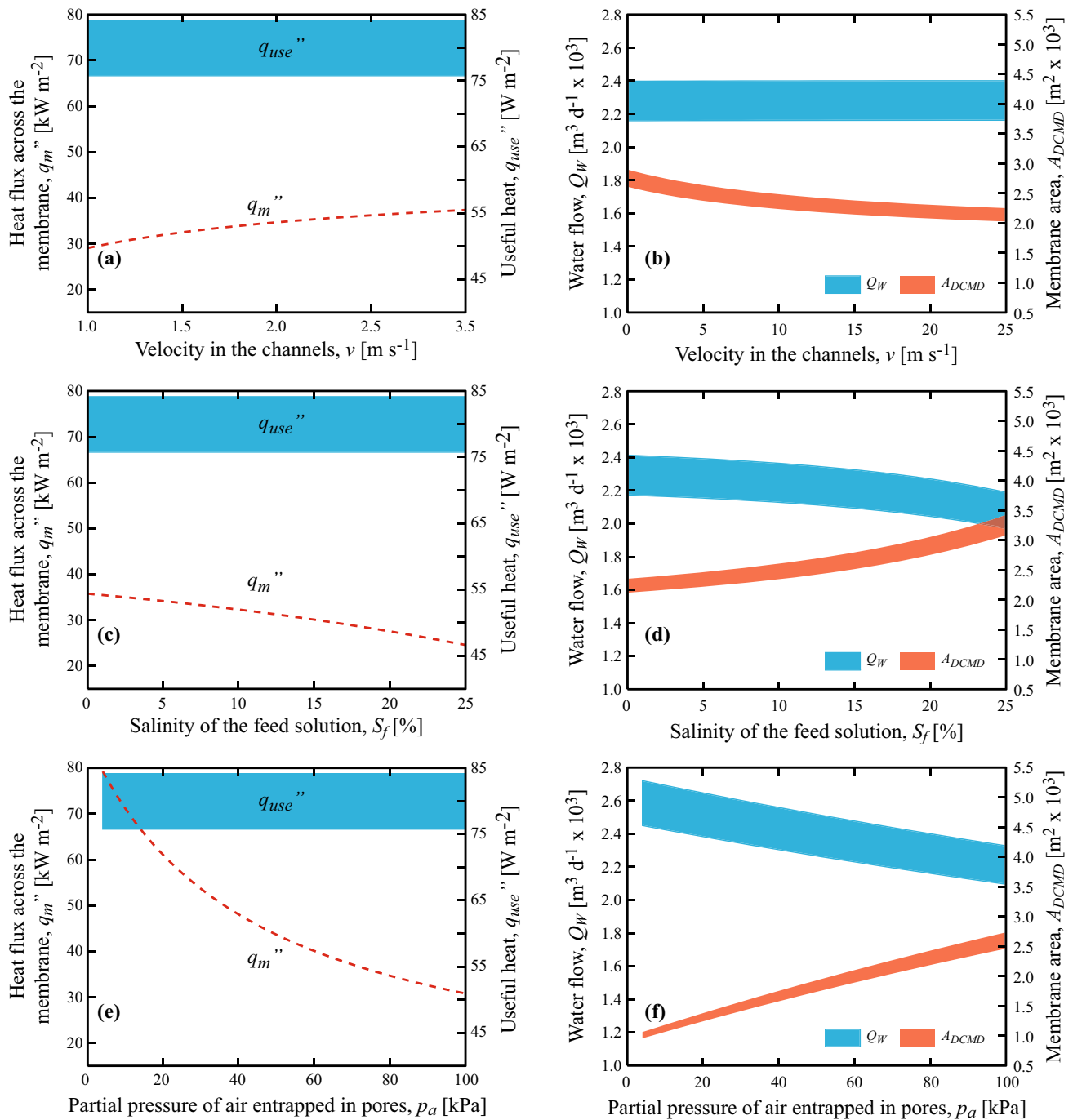


Fig. 5 **a** Influence of the velocity in the membrane channels (v) on the heat flux across the membrane (q_m'') and on the useful heat that can be collected from the pond (q_{USE}''). **b** Influence of the velocity in the membrane channels on the freshwater produced (Q_W) and on the membrane area (A_{DCMD}). **c** Effect of the salinity of the feed solution (S_f) on the heat flux across the membrane and on the useful heat that can be collected from the pond. **d** Effect of the salinity of the feed solution on the freshwater produced and on the membrane area.

e Influence of the partial pressure of air entrapped in the membrane pores (p_a) on the heat flux across the membrane and on the useful heat that can be collected from the pond. **f** Effect of the partial pressure of air entrapped in the membrane pores and on the freshwater produced and on the membrane area. The lower and upper boundaries of q_{USE}'' , Q_W and A_{DCMD} were calculated with the percentile 50th and 90th of the meteorological data observed in Darwin (Australia)

Figure 6 shows the impact of the heat exchanger effectiveness (ϵ) and of the overall thermal efficiency (η_T) on the useful heat that can be collected from the pond

(q_{USE}''), on the membrane feed temperature (T_f), on the heat flux across the membrane (q_m''), on the freshwater flow (Q_W), and on the membrane area (A_{DCMD}). As shown in

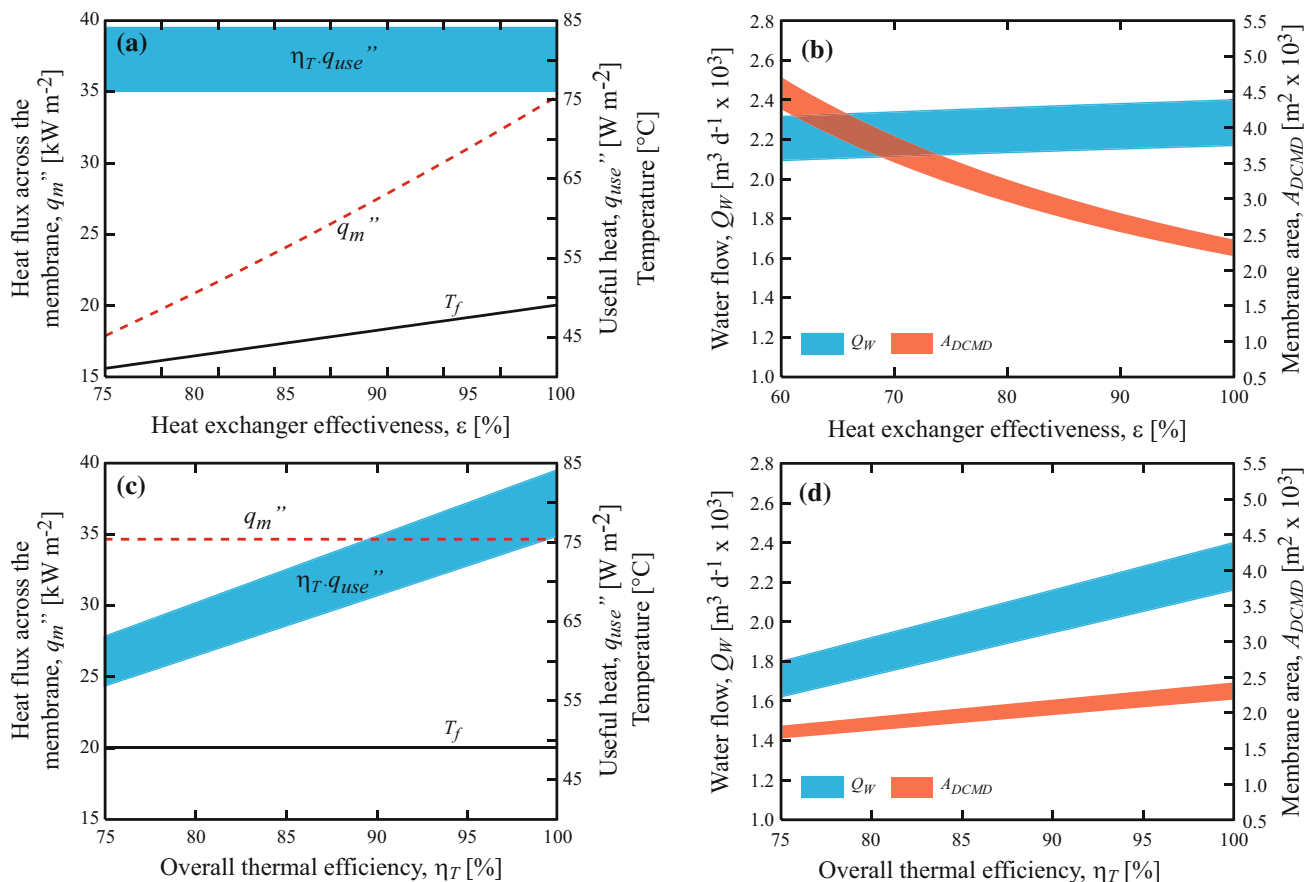


Fig. 6 **a** Effect of the heat exchanger effectiveness on the useful heat that can be collected from the pond, on the feed temperature (T_f) and on the heat flux across the membrane. **b** Effect of the heat exchanger effectiveness on the freshwater produced (Q_W) and on the membrane area (A_{DCMD}). **c** Effect of the overall thermal efficiency on the useful heat that can be collected from the pond, on the feed temperature and

on the heat flux across the membrane. **d** Effect of the overall thermal efficiency on the freshwater produced and on the membrane area. The lower and upper boundaries of the useful heat that can be collected from the pond, the freshwater produced and the membrane area were calculated with the percentile 50th and 90th of the meteorological data observed in Darwin (Australia)

Fig. 6a, as the heat exchanger effectiveness increases both the membrane feed side temperature and the heat flux across the membrane increase, and the useful heat remains constant as it depends on the meteorological conditions and on the temperature of the lower convective zone. Note that as the membrane feed side temperature increases, the heat flux across the membrane also increases because of a larger water flux (latent flux) across the membrane and also due to larger conductive heat losses. To satisfy the first law of thermodynamics, the increase in the heat flux across the membrane has to be accompanied with a reduction in the membrane area (Fig. 6b). Therefore, the final freshwater production remains relatively constant with a slight increase as the heat exchanger effectiveness increases. This increase in the heat exchanger effectiveness would be reflected on capital expenditures more than in revenue due to freshwater production. Also, as explained by Suárez et al. (2010b) and according to the heat capacities of seawater and of the lower convective zone fluid, the heat

exchanger effectiveness most likely will be $\sim 90\%$. On the other hand, when the overall thermal efficiency increases (Fig. 6c), the membrane feed side temperature and the heat flux across the membrane remains constant. Nonetheless, the useful heat collected from the pond increases. To effectively use the additional energy collected from the pond, the membrane area has to increase (Fig. 6d). Therefore, the freshwater flow increases in $\sim 33\%$ when the overall thermal efficiency goes from 75 to 100%. As described before, the laboratory-scale solar pond constructed by Suárez et al. (2015) has an overall thermal efficiency of $\sim 68\%$. Nonetheless, as that pond had many energetic inefficiencies (see Suárez et al. 2014b, 2015), it is expected that outdoor large-scale solar pond would have overall thermal efficiencies larger than 80%. Note that an additional capital expenditure related to enhance the overall thermal efficiency will also result in more revenues due to freshwater production (as opposed to the previous situation).

Other energy requirements for DCMD driven by solar ponds are the pumping energy to circulate the fluids throughout the system and the energy needed to reduce the partial pressure of air entrapped in the membrane pores. According to Suárez et al. (2010b), as DCMD operates near atmospheric pressure, the pumps only need to overcome frictional and singular head losses, which are on the order of 1 % or less of the useful energy collected in the solar pond. On the other hand, as described by Cabassud and Wirth (2003), the energy needed to create a vacuum of less than 5 kPa in an MD system is on the order of 1 kWh per m³ of freshwater produced, which is less than 0.1 % of the solar pond useful energy (Suárez et al. 2010b). Therefore, these additional energetic requirements are negligible compared to the energy that can be extracted from the solar pond.

Conclusions

Water and energy are fundamentally linked and are crucial for sustainable development. Desalination has been one solution for water production but still requires large amounts of energy. Nonetheless, desalination driven by solar energy is an attractive solution to tackle this water-energy nexus. In this work, the performance of a DCMD system driven by solar ponds was investigated. With this aim, a mathematical model was constructed and validated using experimental data available in the scientific literature.

The worldwide spatial distribution of useful heat in the solar pond and water produced in the membrane distillation module were assessed using global meteorological data, the results obtained from the experiments, and the heat and mass transfer model developed to study this coupled system. This assessment allows determining the best settings for solar pond operation. It was found that zones near the ocean between 40°N and 40°S are ideal locations for solar pond development because they have enough solar radiation, and availability of excess water and salts to operate this system. For inland zones with excess water and salts, this coupled system must be combined with evaporation ponds to reduce its environmental footprint.

The maximum water production values that can be obtained are on the order of 3.0 L d⁻¹ per m² of solar pond (12.1 m³ d⁻¹ acre⁻¹), but the expected water production values are more likely to be on the order of 2.5 L d⁻¹ per m² of solar pond (10.1 m³ d⁻¹ acre⁻¹) when the system operates with inefficiencies. The coupled system has a thermal energy consumption of 880 ± 60 kWh per m³ of distillate, which is within the range of other membrane distillation systems powered by solar energy. Given the thermal energy consumption of this system, a careful sizing

of the membrane area, in terms of the dimensions of the solar pond, has to be conducted. Our results show that the membrane area has to be 1000 times smaller than the area of the solar pond to achieve continuous and, thus, sustainable operation.

The effect of operational conditions, such as the velocity in the membrane channels, the partial pressure of air entrapped in the membrane pores, and the feed solution salinity, on the performance of the system was evaluated. The most important operating parameters that influence the freshwater production rates are the partial pressure of air entrapped in the membrane pores and the overall thermal efficiency of the coupled system. The results of this work can be used as a guide for geographical zone selection and operation of a membrane distillation system driven by solar ponds that can help mitigate the stress on the water-energy nexus.

Acknowledgments The authors wish to thank the Comisión Nacional de Investigación Científica y Tecnológica (CONICYT), Chile, for funding project Fondecyt de Iniciación N°11121208, the Centro de Desarrollo Urbano Sustentable (CEDEUS—CONICYT/FONDAP/15110020), and the Center for Solar Energy Technologies (CSET—CORFO CEI2-21803). The authors also want to thank the editor and the four anonymous reviewers that provided many thoughtful comments that improved this manuscript.

References

- Al-Obaidani S, Curcio E, Macedonio F, Di Profio G, Al-Hinai H, Drioli E (2008) Potential of membrane distillation in seawater desalination: thermal efficiency, sensitivity study and cost estimation. *J Membr Sci* 323:85–98. doi:10.1016/j.memsci.2008.06.006
- Banat F, Jumah R, Garaibeh M (2002) Exploitation of solar energy collected by solar stills for desalination by membrane distillation. *Renew Energy* 25:293–305. doi:10.1016/S0960-1481(01)00058-1
- Blanco Gálvez J, García-Rodríguez L, Martín-Mateos I (2009) Seawater desalination by an innovative solar-powered membrane distillation system: the MEDESOL project. *Desalination* 246:567–576. doi:10.1016/j.desal.2008.12.005
- Cabassud C, Wirth D (2003) Membrane distillation for water desalination: how to choose an appropriate membrane? *Desalination* 157:307–314. doi:10.1016/S0011-9164(03)00410-7
- Camacho LM, Dumée L, Zhang J, Li J-d, Duke M, Gomez J, Gray S (2013) Advances in membrane distillation for water desalination and purification applications. *Water* 5:94–196. doi:10.3390/w5010094
- Cath T, Adams V, Childress AE (2004) Experimental study of desalination using direct contact membrane distillation: a new approach to flux enhancement. *J Membr Sci* 228:5–16. doi:10.1016/j.memsci.2003.09.006
- Curcio E, Drioli E (2005) Membrane distillation and related operations—a review. *Sep Purif Rev* 34:35–86. doi:10.1081/SPM-200054951
- Date A, Yaakob Y, Date A, Krishnapillai S, Akbarzadeh A (2013) Heat extraction from non-convective and lower convective zones of the solar pond: a transient study. *Sol Energy* 97:517–528. doi:10.1016/j.solener.2013.09.013

- Department of Civil and Environmental Engineering/Princeton University (2006) Global meteorological forcing dataset for land surface modeling. <http://rda.ucar.edu/datasets/ds314.0/>. Research Data Archive at the National Center for Atmospheric Research, Computational and Information Systems Laboratory, Boulder. Accessed 5 May 2016
- Drioli E, Ali A, Macedonio F (2015) Membrane distillation: recent developments and perspectives. *Desalination* 356:56–84. doi:10.1016/j.desal.2014.10.028
- Emec S, Bilge P, Seliger G (2015) Design of production systems with hybrid energy and water generation for sustainable value creation. *Clean Technol Environ Policy* 17:1807–1829. doi:10.1007/s10098-015-0947-4
- Gilron J (2014) Water-energy nexus: matching sources and uses. *Clean Technol Environ Policy* 16:1471–1479. doi:10.1007/s10098-014-0853-1
- González D, Amigo J, Lorente S, Bejan A, Suárez F (2016) Constructal Design of salt-gradient solar pond fields. *Int J Energy Res*. doi:10.1002/er.3539
- Hickenbottom KL, Cath TY (2014) Sustainable operation of membrane distillation for enhancement of mineral recovery from hypersaline solutions. *J Membr Sci* 454:426–435. doi:10.1016/j.memsci.2013.12.043
- Hull JR, Nielsen CE, Golding P (1989) *Salinity-gradient solar ponds*. CRC Press, Boca Raton
- Karagiannis I, Soldatos PG (2008) Water desalination cost literature: review and assessment. *Desalination* 223:448–456. doi:10.1016/j.desal.2007.02.071
- Khayet M (2013) Solar desalination by membrane distillation: dispersion in energy consumption analysis and water production costs (a review). *Desalination* 308:89–101. doi:10.1016/j.desal.2012.07.010
- Koschikowski J, Wiegand M, Rommel M, Ortin VS, Suarez BP, Betancort Rodríguez JR (2009) Experimental investigations on solar driven stand-alone membrane distillation systems for remote areas. *Desalination* 248:125–131. doi:10.1016/j.desal.2008.05.047
- Leblanc J, Akbarzadeh A, Andrews J, Lu H, Golding P (2011) Heat extraction methods from salinity-gradient solar ponds and introduction of a novel system of heat extraction for improved efficiency. *Sol Energy* 85(3103–3142):2011. doi:10.1016/j.solener.2010.06.005
- Li C, Goswami Y, Stefanakos E (2013) Solar assisted seawater desalination: a review. *Renew Sustain Energy Rev* 19:136–163. doi:10.1016/j.rser.2012.04.059
- Lu H, Walton J, Swift A (2001) Desalination coupled with salinity-gradient solar ponds. *Desalination* 136:13–23. doi:10.1016/S0011-9164(01)00160-6
- Lu H, Swift AP, Hein HD, Walton JC (2004) Advancements in salinity gradient solar pond technology based on sixteen years of operational experience. *J Sol Energy Eng* 126:759–767. doi:10.1115/1.1667977
- Martinetti CR, Childress AE, Cath TY (2009) High recovery of concentrated RO brines using forward osmosis and membrane distillation. *J Membr Sci* 331:31–39. doi:10.1016/j.memsci.2009.01.003
- Martinez L, Rodriguez-Maroto JM (2006) Characterization of membrane distillation modules and analysis of mass flux enhancement by channel spacers. *J Membr Sci* 274:123–137. doi:10.1016/j.memsci.2005.07.045
- Mathioulakis E, Belessiotis V, Delyannis E (2007) Desalination by using alternative energy: review and state-of-the-art. *Desalination* 203:346–365. doi:10.1016/j.desal.2006.03.531
- Mericq J-P, Laborie S, Cabassud C (2011) Evaluation of systems coupling vacuum membrane distillation and solar energy for seawater desalination. *Chem Eng J* 166:596–606. doi:10.1016/j.cej.2010.11.030
- Nakoa K, Rahaoui K, Date A, Akbarzadeh A (2015) An experimental review on coupling of solar pond with membrane distillation. *Sol Energy* 119:319–331. doi:10.1016/j.solener.2015.06.010
- Nasr P, Sewilam H (2015) Forward osmosis: an alternative sustainable technology and potential applications in water industry. *Clean Technol Environ Policy* 17:2079–2090. doi:10.1007/s10098-015-0927-8
- Nie Z, Bu L, Zheng M, Huang W (2011) Experimental study of natural brine solar ponds in Tibet. *Sol Energy* 85:1537–1542. doi:10.1016/j.solener.2011.04.011
- Phattaranawik J, Jiratananon R, Fane AG (2003) Heat transport and membrane distillation coefficients in direct contact membrane distillation. *J Membr Sci* 212:177–193. doi:10.1016/S0376-7388(02)00498-2
- Rabl A, Nielsen C (1975) Solar ponds for space heating. *Sol Energy* 17:1–12. doi:10.1016/0038-092X(75)90011-0
- Ranjan KR, Kaushik SC (2014) Exergy analysis of the active solar distillation systems integrated with solar ponds. *Clean Technol Environ Policy* 16:791–805. doi:10.1007/s10098-013-0669-4
- Ruskowitz JA, Suárez F, Tyler SW, Childress AE (2014) Evaporation suppression and solar energy collection in a salt-gradient solar pond. *Sol Energy* 99:36–46. doi:10.1016/j.solener.2013.10.035
- Safavi M, Mohammadi T (2009) High-salinity water desalination using VMD. *Chem Eng J* 149:191–195. doi:10.1016/j.cej.2008.10.021
- Saleh A, Qudeiri JA, Al-Nimr MA (2011) Performance investigation of a salt gradient solar pond coupled with desalination facility near the Dead Sea. *Energy* 36:922–931. doi:10.1016/j.energy.2010.12.018
- Seckler D, Barker R, Amarasinghe U (1999) Water scarcity in the twenty-first century. *Int J Water Resour Dev* 15(1–2):29–42. doi:10.1080/07900629948916
- Shannon MA, Bohn PW, Elimelech M, Georgiadis JG, Mariñas BJ, Mayes AM (2008) Science and technology for water purification in the coming decades. *Nature* 452:301–310. doi:10.1038/nature06599
- Solis S (1999) Water desalination by membrane distillation coupled with a solar pond. Ms. Thesis, University of Texas at El Paso
- Suárez F, Tyler SW, Childress AE (2010a) A fully coupled transient double-diffusive convective model for salt-gradient solar ponds. *Int J Heat Mass Transf* 53(9–10):1718–1730. doi:10.1016/j.ijheatmasstransfer.2010.01.017
- Suárez F, Tyler SW, Childress AE (2010b) A theoretical study of a direct contact membrane distillation system coupled to a salt-gradient solar pond for terminal lakes reclamation. *Water Res* 44(15):4601–4615. doi:10.1016/j.watres.2010.05.050
- Suárez F, Childress AE, Tyler SW (2010c) Temperature evolution of an experimental salt-gradient solar pond. *J Water Clim Change* 1(4):246–250. doi:10.2166/wcc.2010.101
- Suárez F, Aravena JE, Hausner MB, Childress AE, Tyler SW (2011) Assessment of a vertical high-resolution distributed-temperature-sensing system in a shallow thermohaline environment. *Hydrol Earth Syst Sci* 15(3):1081–1093. doi:10.5194/hess-15-1081-2011
- Suárez F, Muñoz JF, Fernández B, Dorsaz JM, Hunter CK, Karavatis CA, Gironás J (2014a) Integrated water resource management and energy requirements for water supply in the Copiapó river basin, Chile. *Water* 6:2590–2613. doi:10.3390/w6092590
- Suárez F, Ruskowitz JA, Childress AE, Tyler SW (2014b) Understanding the expected performance of large-scale solar ponds from laboratory-scale observations. *Appl Energy* 117:1–10. doi:10.1016/j.apenergy.2013.12.005

- Suárez F, Ruskowitz JA, Tyler SW, Childress AE (2015) Renewable water: direct contact membrane distillation coupled with solar ponds. *Appl Energ* 158:532–539. doi:[10.1016/j.apenergy.2015.08.110](https://doi.org/10.1016/j.apenergy.2015.08.110)
- Vásquez C, Ortiz C, Suárez F, Muñoz JF (2013) Modeling flow and reactive transport to explain mineral zoning in the Salar de Atacama aquifer, Chile. *J Hydrol* 490:114–125. doi:[10.1016/j.jhydrol.2013.03.028](https://doi.org/10.1016/j.jhydrol.2013.03.028)
- Yun YB, Ma RY, Zhang WZ, Fane AG, Li JD (2006) Direct contact membrane distillation mechanism for high concentration NaCl solutions. *Desalination* 188:251–262. doi:[10.1016/j.desal.2005.04.123](https://doi.org/10.1016/j.desal.2005.04.123)